Structure and far-infrared edge modes of quantum antidots at zero magnetic field

A. Emperador[1], M. Pi[1], M. Barranco[1], E. Lipparini[2], and Ll. Serra[3].
[1]*Departament d'Estructura i Constituents de la Matèria, Facultat de Física, Universitat de Barcelona, E-08028 Barcelona, Spain*
[2]*Dipartimento di Fisica, Università di Trento. 38050 Povo, Italy*
[3]*Departament de Física, Facultat de Ciències, Universitat de les Illes Balears, E-07071 Palma de Mallorca, Spain*
(February 7, 2008)

Abstract

We have investigated edge modes of different multipolarity sustained by quantum antidots at zero magnetic field. The ground state of the antidot is described within a local density functional formalism. Two sum rules, which are exact within this formalism, have been derived and used to evaluate the energy of edge collective modes as a function of the surface density and the size of the antidot.

PACS 73.20.Dx, 73.20.Mf, 78.20.Bh

With the progress of microstructure technology, the study of the two dimensional electron gas (2DEG) has evolved to that of laterally confined superlattices made of either electron islands (dots) or holes surrounded by electrons (antidots). Much effort has been devoted in the past to the study of quantum dots, as compared to that put in the study of quantum antidots. One of the goals of their study has been to determine the far-infrared response of these semiconductor microstructures, and the formation of compressible and incompressible states when a magnetic field B is perpendicurlaly applied. In the case of antidots, which is the subject of the present work, experimental evidence of collective excitations sustained by these structures has been presented in Refs. [1–3]. A theoretical description based on magnetoplasmons in two-dimensional antidot structures has been given in Ref. [4] which compares well with the experimental data of Ref. [2]. Recently, the existence of compressible and incompressible strips at the edge of antidots has been determined by far-infrared spectroscopy [5].

We have started a systematic study of the structure and collective far-infrared response of antidots, whose aim is to achieve a level of sophistication in the description of these systems similar to that attained for quantum dots. As a first step, we present here results at zero magnetic field obtained within Density Functional Theory (DFT). To some extend, the present study is similar in scope to that carried out in Ref. [6] on the surface excitations of cavities in 3D metals. The $B \neq 0$ case, which requires a rather different and far more complex approach, will be presented in a forthcoming paper.

We have modelled an antidot of radius R in a 2DEG of surface density n_s by a positive jellium background of density $n_s\,\Theta(r-R)$ to which we have added for the reason that will be given below, a parabolic potential barrier of the type $V_p(r) = m^*\omega_0^2(R^2-r^2)/2$ acting on the electrons for $r \leq R$. We shall call V_{ext} the sum of the jellium and V_p potentials. The ground state (gs) of the antidot is obtained solving the Kohn-Sham (KS) equations as indicated for example in Ref. [7]. The problem is simplified by the imposed circular symmetry, and only the radial KS equations have to be considered to determine the electronic radial wave functions $R_l(r)$:

$$\frac{d^2R_l(r)}{dr^2} + \frac{1}{r}\frac{dR_l(r)}{dr} + \left[\frac{2m^*}{\hbar^2}\left(E - V(r)\right) - \frac{l^2}{r^2}\right] R_l(r) = 0 \ , \tag{1}$$

where m* is the electron effective mass which together with a dielectric constant ϵ are characteristics of the semiconductor. For example, $\epsilon = 12.4$ and m$^* = 0.067$ m$_e$ in GaAs, which we have chosen for the numerical applications in view of the existing experimental data of Refs. [2,5]. $l = 0, \pm1, \pm2...$ is the angular momentum about the z axis perpendicular to the plane of the antidot, and r is the radial variable in that plane. The single electron potential $V(r)$ is made of V_{ext}, of the Hartree electron-electron potential and of the exchange-correlation potential. The correlation potential has been obtained from the correlation energy of Ref. [8] in a local density approximation. Some times we shall use effective atomic units. In this system of units, the length unit is the Bohr radius times ϵ/m^*, and the energy unit is the Hartree times m^*/ϵ^2, denoted here as a_0^* and H^*, respectively. ϵ is the dielectric

constant, and $m = m^* m_e$ is the electron effective mass. For GaAs we have ϵ=12.4 and m^*=0.067. Consequently, $a_0^* \sim 97.9$Å and $H^* \sim 11.9$ meV ~ 95.6 cm^{-1}.

Physically acceptable solutions to Eq. (1) have to be regular at $r = 0$ and behave asymptotically as $R_l(r,k) \sim J_l(kr) + tan(\delta_l) Y_l(kr)$, where J_l and Y_l are the integer Bessel functions of first and second kind [9], and $k = \sqrt{2m^*(E - V_\infty)/\hbar^2}$. The wave number k has to be $k \leq k_F = \sqrt{2\pi n_s}$. Taking into consideration the spin degeneracy, the electron density $\rho(r)$ is obtained as

$$\rho(r) = \sum_{l=-\infty}^{l=\infty} \frac{2}{(2\pi)^2} \int_{|\vec{k}| \leq k_F} R_l^2(r,k)\, d\,\vec{k} \ . \tag{2}$$

We have checked that the number of points used to carry out a Gaussian integration over k, and the maximum $|l|$ employed in Eq. (2) lead to stable results. Typically, some 1000-1500 wave functions have been computed to obtain a density.

We show in Fig. (1) the electronic densities corresponding to antidots of $R = 7.5\ a_0^*$ and n_s = 0.05, 0.1, 0.2, 0.3 and 0.4 $(a_0^*)^{-2}$. They span the size and density range of those fabricated and experimentally studied in Ref. [2], and have been obtained using $\omega_0 = 0.09 H^*$. Figure (2) shows the $V(r)$ KS potential corresponding to $n_s = 0.1$ and 0.4 $(a_0^*)^{-2}$. Also indicated are the Fermi energy and the contribution of $V_p(r)$ to $V(r)$.

Looking at the position of the Fermi energy with respect of the top of $V(r)$, it is not surprising that a potential barrier of a kind or another is needed to prevent the electrons from spilling in the antidot too much, producing an unphysical representation of the experimental device. Actually, we have found that if ω_0 is set to zero, high density antidots would have non-zero electron densities even at $r = 0$. This is illustrated in Fig. (3) for the $R = 180$ nm, $n_s = 9 \times 10^{11}$ cm^{-2} antidot of Ref. [5]. In this figure, the dashed line density has been obtained setting $\omega_0 = 0$.

These results can be employed to determine the $B = 0$ far-infrared multipole response of antidots. To do so, we rely on the formalism described in detail in Ref. [10]. For the present purpose, it consists in obtaining the so-called m_1 and m_3 sum rules (SR) for an excitation operator Q_L. We have that [11]:

$$\begin{aligned} m_1(Q_L) &= \frac{1}{2} \langle 0 | [Q_L^+, [H, Q_L]] | 0 \rangle \\ m_3(Q_L) &= \frac{1}{2} \langle 0 | [[H, [H, Q_L^+]], [H, Q_L]] | 0 \rangle \ , \end{aligned} \tag{3}$$

where $|0\rangle$ is the gs of the system. These SR have been extensively studied in the literature [11,12]. As indicated in these references, if only a collective state is contributing to the strenght function, $E_3(Q_L) \equiv (m_3/m_1)^{1/2}$ represents the average excitation energy. This is the situation experimentally found for antidots at zero magnetic field.

The operator Q_L is taken to be

$$Q_L = \sum_{j=1}^{N} \frac{1}{r_j^L}\, e^{iL\theta_j} \ . \tag{4}$$

This choice is inspired in that $(qr)^{-L}e^{iL\theta}$ is the small q expansion of the function $Y_L(qr)e^{iL\theta}$, which is the restriction to the $z=0$ plane of the irregular solution of the Laplace equation in cylindrical coordinates. Following Ref. [10], a lengthy but straightforward calculation yields:

$$m_1(Q_L) = 2\pi L^2 \int_0^\infty dr\, \frac{1}{r^{2L+1}}\, \rho(r) \tag{5}$$

$$m_3(Q_L) = m_3(T) + m_3(ee) + m_3(V_{ext}\, e) \ , \tag{6}$$

where

$$m_3(T) = 2\pi L^2(L+1) \int_0^\infty dr\, \frac{1}{r^{2L+3}}\, [L\tau(r) + 2(L+2)\lambda(r)] \tag{7}$$

$$\begin{aligned} m_3(ee) = {} & 4\pi L^2 \frac{(2L-1)!!}{2^L\, L!} \int_0^\infty \rho'(r) dr \left\{ \frac{1}{r^{2L+1}} \int_0^r \left[2\rho'(r') + r'\rho''(r')\right] E_L\left(\frac{r'}{r}\right) dr' \right. \\ & + \left. \int_r^\infty \frac{1}{r'^{(2L+1)}} \left[(2L+1)\rho'(r') - r'\rho''(r')\right] E_L\left(\frac{r}{r'}\right) dr' - \frac{2^{L+1}L!}{(2L+1)!!} \frac{1}{r^{2L}} \rho'(r) \right\} \\ & + 4\pi L^2 \int_0^\infty dr\, \frac{1}{r^{2L+2}} \left[r\rho''(r) - (2L+1)\rho'(r)\right] \left\{ \frac{1}{r} \int_0^r \left[3r'\rho(r') + r'^2\rho'(r')\right] \mathbf{E}\left(\frac{r'}{r}\right)\, dr' \right. \\ & - \left. \int_r^\infty r'\rho'(r') \mathbf{E}\left(\frac{r}{r'}\right)\, dr' - 2\, r\rho(r) + \lim_{R_\infty \to \infty} R_\infty n_s \mathbf{E}\left(\frac{r}{R_\infty}\right) \right\} \end{aligned} \tag{8}$$

$$m_3(V_{ext}\, e) = \pi L^2 \int_0^\infty dr V_{ext}(r) \left[\rho''(r) - \frac{2L+1}{r}\rho'\right] \frac{1}{r^{2L+1}} \ . \tag{9}$$

The definition of the densities $\tau(r)$ and $\lambda(r)$ and of the function E_L can be found in Ref. [10], and the primes on the density denote r-derivatives. The jellium potential $V_+(r)$ entering in V_{ext} is:

$$V_+(r) = 4n_s \begin{cases} R_\infty\, \mathbf{E}(r/R_\infty) - R\, \mathbf{E}(r/R) & r < R \\ R_\infty\, \mathbf{E}(r/R_\infty) - r\, \mathbf{E}(R/r) + r\, (1 - (R/r)^2)\, \mathbf{K}(R/r) & r > R \ . \end{cases} \tag{10}$$

In the above equations, $\mathbf{K}$ and $\mathbf{E}$ are the complete elliptic integrals of first and second kind, respectively [13], and R_∞ represents a large r value. In practice, it is the largest r used in the structure calculation, which we have also taken as the point where the asymptotic behavior of $R_l(r)$ holds. We want to point out that the two Coulomb diverging terms in $m_3(ee)$ and $m_3(V_{ext}\, e)$ cancel each other.

The present formalism can be applied to antidots with the restriction that $\rho(r)$ vanishes in a small disk around the origin. In practice, this is not a limitation, as can be inferred from Figs. (1,3) (see also Fig. 5). Some technical details about how the above integrals are handle can be found in Sec. IV of Ref. [6].

For a large antidot, the electronic density is constant everywhere apart from a narrow region along the border of the hole. Following the method outlined in Ref. [10], it is easy to show that E_3 yields the classical hydrodynamics dispersion relation for edge waves, namelly

$E_3 = \omega(q) \sim \sqrt{2\, n_s\, q\, \ln(q_0/q)}$. It is also worth to notice that the induced (or transition) density associated to the operator Q_L has the form [10]

$$\rho_{tr}(\vec{r}) \propto L \frac{1}{r^{L+1}}\, \rho'(r) \tag{11}$$

that manifests the edge character of the excitation.

Figure (4) shows the frequency of the $L = 1$ mode as a function of n_s compared with the experimental points of [2]. For completeness, we have also plotted the results corresponding to $L = 2$. We have checked that similar results are obtained using as potential barrier the parabola $V_p(r) = m^* \omega_0^2 (R-r)^2/2$ for $r \leq R$ with $\omega_0 = 1 H^*$. One can see that the agreement with experiment is good. Furthermore, our calculation yields a frequency of ~ 68 cm^{-1} for the $R = 180$ nm, $n_s = 9 \times 10^{11}$ cm^{-2} antidot, in good agreement with the experimental findings of Ref. [5].

We have also studied the size dependence of the mode energy. Fig. (5) represents the electronic densities for antidots of $R = 10$, 15 and 20 a_0^*, and a surface density $n_s = 0.2$ $(a_0^*)^{-2}$. The frequencies of the $L = 1$ and 2 modes are shown in Fig. (6) as a function of $1/\sqrt{R}$. They exhibit a distinct R dependence, indicating a clear departure from parabolicity of the confining potential, i.e., a physical situation where the generalized Kohn theorem does not apply.

If the electronic density $\rho(r)$ is approximated by a quasi-step function, an analytical expression can be obtained for E_3^2. Proceeding as in Ref. [10] one gets:

$$E_3^2 = \pi n_s \frac{L(L+1)}{R^2} + 4 n_s \frac{L}{R} \left[\frac{1}{2}\, ln\, \left(\gamma \frac{R}{a} \right) + 1 - \sum_{m=1}^{L} \frac{1}{2m-1} \right] \ , \tag{12}$$

where a represents the width of the quasi-step function, and the precise value of γ depends on the way the electronic density goes to zero [14]. This equation tells one that the frequencies have a $1/\sqrt{R}$ linear dependence if the Coulomb energy contribution dominates. For reasonable values of γ/a, it happens for any realistic value of R.

Equation (12) is too crude an approximation because of the quasi-step function density used to get it. Much better results can be obtained if Eqs. (5-9) are evaluated in the Thomas-Fermi approximation, i.e. $\tau(r) = \pi \rho^2(r)$, $\lambda(r) = \tau(r)/2$ [10], after having fitted the KS density to a generalized Fermi function of the kind

$$\rho(r) = n_s \left(1 - \frac{1}{1 + e^{(r-R)/a}} \right)^{\nu} \ . \tag{13}$$

For $n_s = 0.2$ $(a_0^*)^{-2}$, the KS densities are well reproduced on average taking $\nu = 1.1$ and a $= 0.38$ a_0^* (see Fig. 5). The mode frequencies are represented by the lines in Fig. (6).

In conclusion, we have shown that Density Functional Theory is able to reproduce the zero magnetic field frequency of antidot edge modes in quite a similar way as it does for quantum dots. Although a satisfactory description of the collective spectrum of antidots can be achieved using a magnetoplasmon approach [4], an alternative method based on a more microscopic approach such as DFT is needed to discuss other interesting problems, such as edge reconstruction and the formation of compressible and incompressible strips at the antidot edge [5].

It is a pleasure to thank Ricardo Mayol and Francesc Salvat for useful discussions. This work has been performed under grants PB95-1249 and PB95-0492 from CICYT, Spain, and GRQ94-1022 from Generalitat of Catalunya. A.E. acknowledges support from the Dirección General de Enseñanza Superior (Spain).

REFERENCES

[1] K. Kern, D. Heitmann, P. Grambow, Y. H. Zhang, and K. Ploog, Phys. Rev. Lett. **66**, 1618 (1991).

[2] Y. Zhao, D. C. Tsui, M. Santos, M. Shayegan, R. A. Ghanbari, D. A. Antoniadis, and H. I. Smith, Appl. Phys. Lett **60**, 1510 (1992).

[3] A. Lorke, I. Jejina, and J. P. Kotthaus, Phys. Rev. B **46**, 12845 (1992).

[4] G. Y. Wu and Y. Zhao, Phys. Rev. Lett. **71**, 2114 (1993).

[5] K. Bollweg, T. Kurth, D. Heitmann, V. Gudmundsson, E. Vasiliadou, P. Grambow, and K. Ebert, Phys. Rev. Lett. **76**, 2774 (1996).

[6] Ll. Serra, F. Garcias, J. Navarro, N. Barberán, M. Barranco, and M. Pi, Phys. Rev. B **46**, 9369 (1992).

[7] M. Ferconi and G. Vignale, Phys. Rev. B **50**, 14 722 (1994).

[8] B. Tanatar and D. M. Ceperly, Phys. Rev. B **39**, 5005 (1989).

[9] M. Abramowitz and I. A. Stegun, *Handbook of Mathematical Functions* (Dover Pu., New York, 1970).

[10] E. Lipparini, N. Barberán, M. Barranco, M. Pi, and Ll. Serra, Phys. Rev. B **56**, 12375 (1997).

[11] E. Lipparini and S. Stringari, Phys. Rep **175**, 103 (1989).

[12] O. Bohigas, A.M. Lane, and J. Martorell, Phys. Rep **51**, 267 (1979).

[13] I.S. Gradshteyn and I.M. Ryzhik, *Table of Integrals, Series and Products* (Academic Press, New York, 1980).

[14] S. Giovanazzi, L. Pitaevskii, and S. Stringari, Phys. Rev. Lett. **72**, 3230 (1994).

FIGURES

FIG. 1. Electronic densities as a function of r for antidots of $R = 7.5\ a_0^*$ and $n_s = 0.05$, 0.1, 0.2, 0.3 and 0.4 $(\mathrm{a}_0^*)^{-2}$. Also shown are the jellium densities (dotted lines).

FIG. 2. KS potential $V(r)$ as a function of r for antidots of $R = 7.5\ a_0^*$ and $n_s = 0.1$ and 0.4 $(\mathrm{a}_0^*)^{-2}$ (solid lines). The dashed lines represent $V(r)$ without the $V_p(r)$ contribution. The horizontal solid lines indicate the Fermi level, and the vertical dotted line, the radius of the antidot.

FIG. 3. Same as Fig. 1 for $R = 18.35\ a_0^*$ and $n_s = 0.86\ (a_0^*)^{-2}$. The dashed line density has been obtained setting $\omega_0 = 0$.

FIG. 4. Mode frequency as a function of the electron surface density for $L = 1$ and 2. The crosses are experimental data from Ref. [2], and the lines are drawn to guide the eye.

FIG. 5. Electronic densities as a function of r for antidots of $R = 10$, 15 and 20 a_0^*, and $n_s = 0.2\ (\mathrm{a}_0^*)^{-2}$. Also shown are the jellium densities (dotted lines). The thin solid line represents the parametrized density, Eq. [13], for $R = 20\ a_0^*$.

FIG. 6. $L = 1$ and 2 mode frequencies as a function of $R^{-1/2}$ for $n_s = 0.2\ (\mathrm{a}_0^*)^{-2}$. From right to left, the dots correspond to $R = 7.5$, 10, 12.5, 15, 17.5, and 20 a_0^*. The lines represent the results obtained using the density Eq. [13].

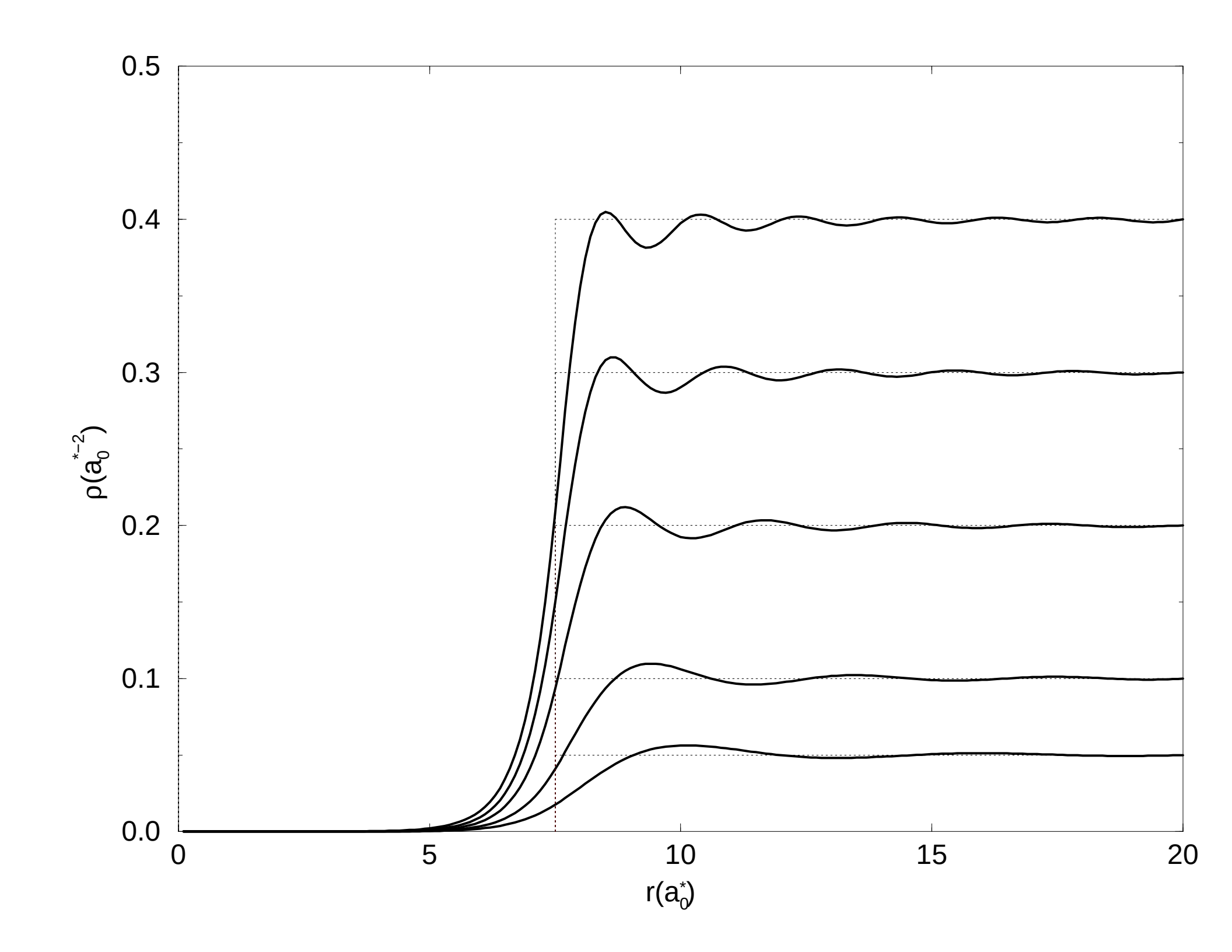
0.5
0.4
0.3
0.2
0.1
0.0
0
5
10
15
20
ρ(a*0−2)
r(a*0)

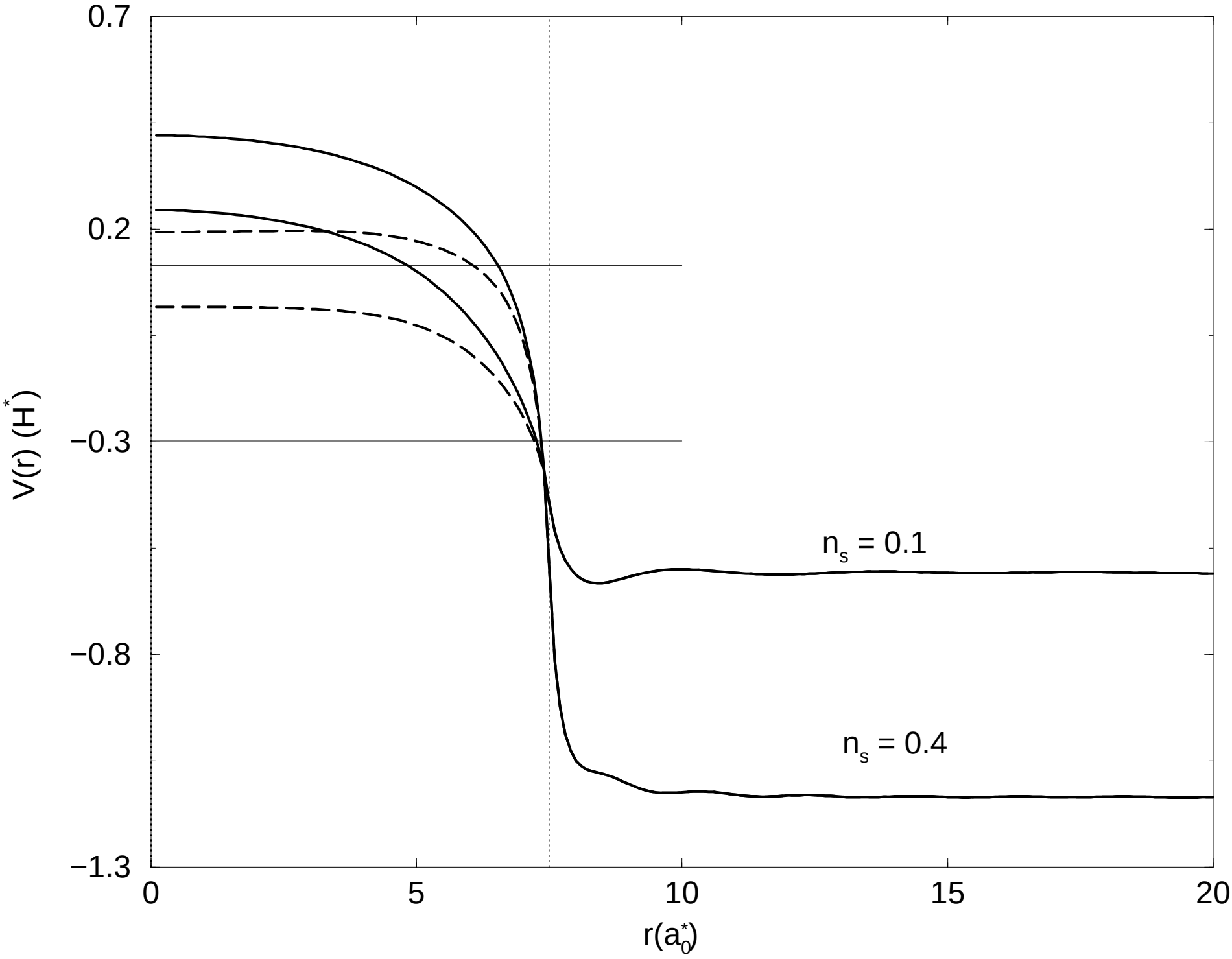
0.7
0.2
−0.3
−0.8
−1.3
0
5
10
15
20
V(r) (H*)
r(a*0)
ns = 0.1
ns = 0.4

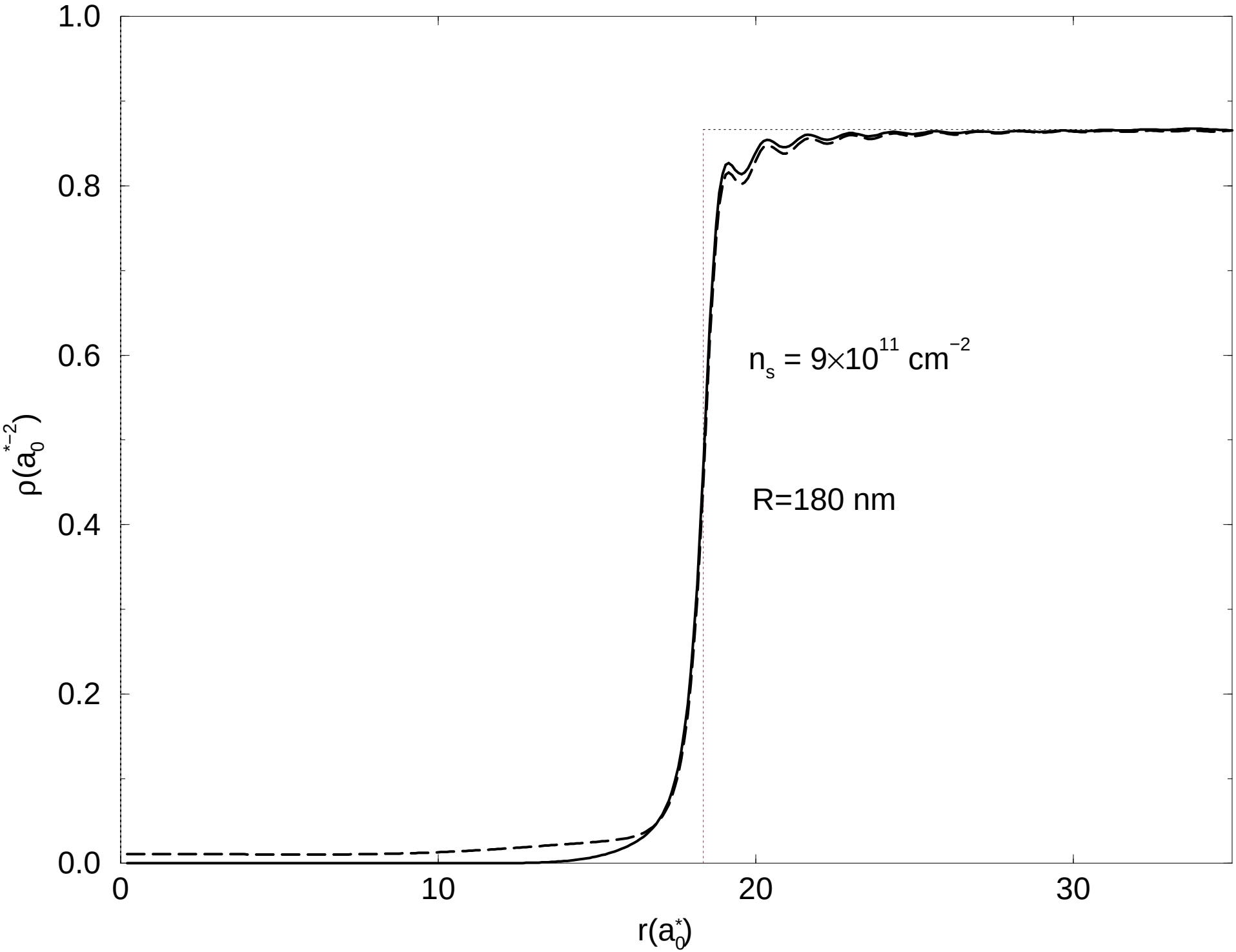
1.0
0.8
0.6
0.4
0.2
0.0
0
10
20
30
ρ(a*0−2)
r(a*0)
ns = 9×10^11 cm^−2
R=180 nm

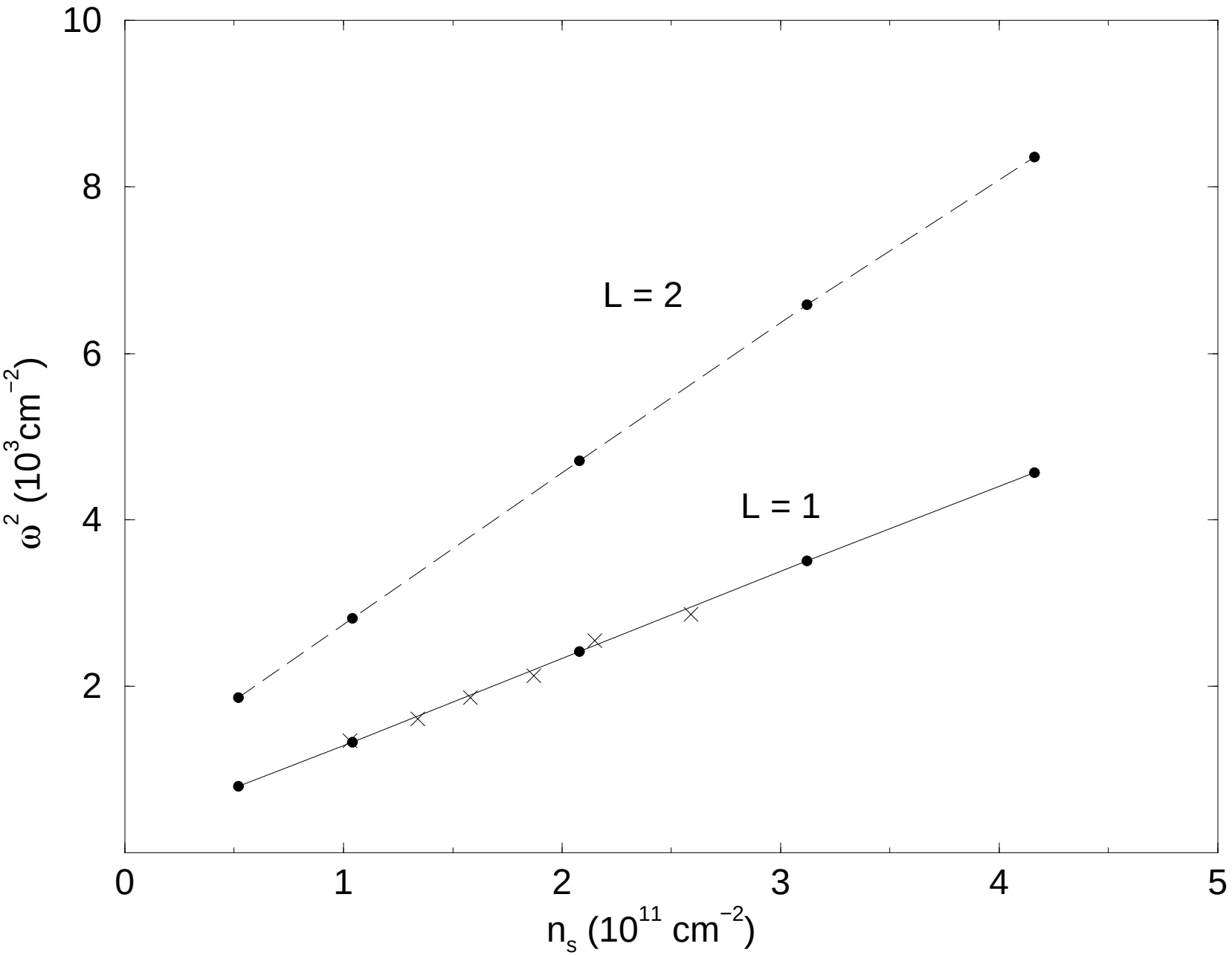
10
8
6
4
2
0
1
2
3
4
5
ω^2 (10^3cm^{-2})
n_s (10^{11} cm^{-2})
L = 2
L = 1

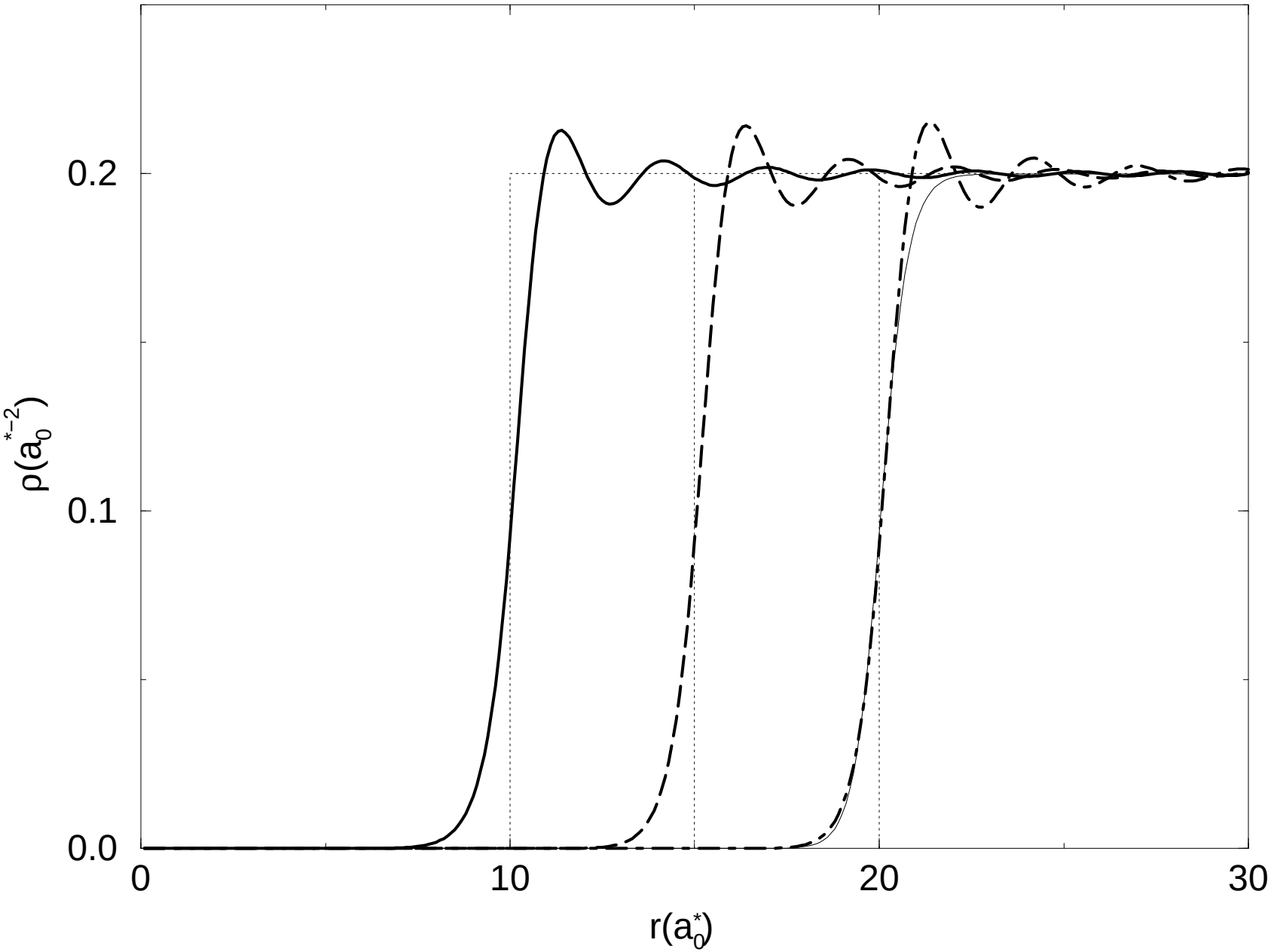
0.2
0.1
0.0
0
10
20
30
ρ(a*0−2)
r(a*0)

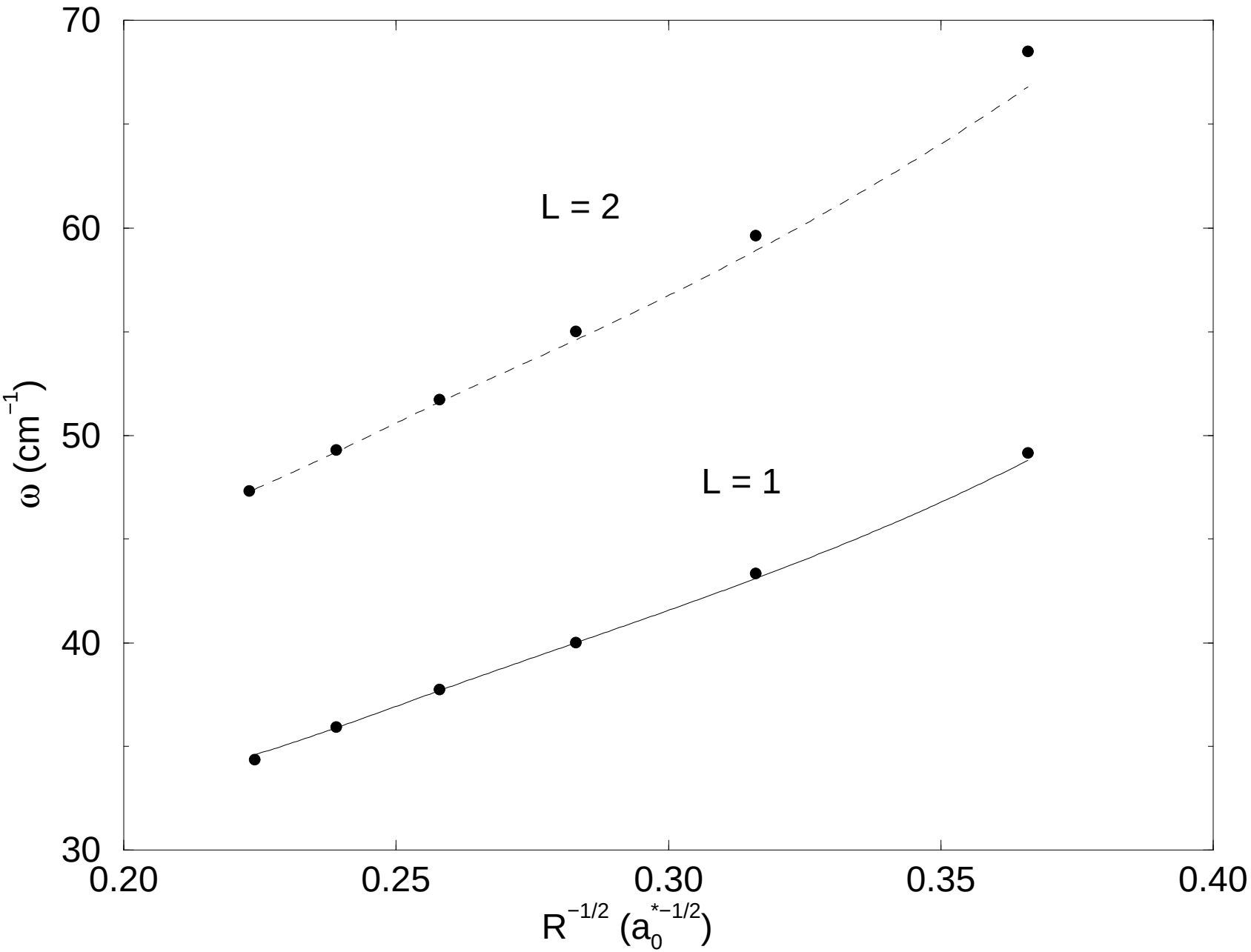
70
60
50
40
30
0.20
0.25
0.30
0.35
0.40
ω (cm^{-1})
R$^{-1/2}$ (a$_0^{*-1/2}$)
L = 2
L = 1